Journal of Alloys and Compounds 489 (2010) 445–450

Contents lists available at ScienceDirect

Journal of Alloys and Compounds

journal homepage: www.elsevier.com/locate/jallcom

Luminescence properties of sol–gel derived $Sr_2(Ce_{1-x}Sn_x)O_4$ blue phosphors

Chia-Hao Hsu, Chia-Lien Liaw, Chung-Hsin Lu*

Department of Chemical Engineering, National Taiwan University, Taipei, Taiwan, ROC

ARTICLE INFO

Article history:
Received 26 March 2009
Received in revised form 24 June 2009
Accepted 25 June 2009
Available online 3 July 2009

Keywords:
Luminescence
Sol–gel
Sn^{4+} ion
LED
Sr_2CeO_4

ABSTRACT

Monophasic $Sr_2(Ce_{1-x}Sn_x)O_4$ phosphors (x = 0–0.07) were prepared via the sol–gel process. A broad excitation band ascribed to the Ce^{4+}–O^{2-} transition was observed in the range of 200–450 nm. With doping Sn^{4+} ions into the host, the intensity of the low-energy peak enhanced remarkably due to a decrease in crystal field. The intensity ratio of the low-energy peak to the high-energy peak increased with the amount of Sn^{4+} ions doped. Moreover, the red shift of the excitation peaks was observed due to an increase in the bond length of Ce–O. Upon excitation at around 346 nm, the intensity of the blue emission peak peaking at 483 nm was enhanced with doping Sn^{4+} ions. The doping of tin ions was found to significantly improve the luminescence characteristics of the prepared phosphors when they were excited under UV light.

1. Introduction

Oxide-based phosphors are widely utilized in various optical devices such as plasma display panels (PDPs), field emission displays (FEDs) and light-emitting diodes (LEDs) due to their high thermal and chemical stability [1]. In recent years, oxide-based lanthanide phosphors have caught much attention because of their excellent optical properties [2]. Comparable red and green emitting phosphors have been widely used in FEDs and LEDs [3–5], but blue emitting phosphors suitable for practical application remain rarely available.

Sr_2CeO_4 was first discovered by Danielson et al. in 1998 [6]. Sr_2CeO_4 phosphor has been confirmed to have an orthorhombic crystal structure with one-dimensional chains of edge-sharing CeO_6 octahedrons linked by strontium ions [7], and it was considered a potential candidate for blue phosphors [8]. In addition, Sr_2CeO_4 was found to emit efficient luminescence under ultraviolet, cathode ray and X-ray excitation [6,9].

Sr_2CeO_4 phosphor displays a broad absorption band in the 200–400 nm range [10]. The broad excitation spectrum in the UV range indicates the feasibility of Sr_2CeO_4 phosphor to be utilized in UV-LEDs. LEDs have become the research and development focus of lighting industry lately and they are widely considered the next generation illumination devices [11,12]. Nishida et al. have shown that the AlGaN-based LEDs emit UV light [13]. When Sr_2CeO_4 phosphors are used for UV-LEDs, they cannot produce strong emission. In this study, in order to improve illumination efficiency of Sr_2CeO_4, tin (IV) ions were used to replace cerium ions in the host in attempt to increase the excitation intensity in the UV range. The photoluminescence properties of the excitation and emission spectra of $Sr_2(Ce_{1-x}Sn_x)O_4$ phosphors were investigated. In addition, the band structure of the prepared phosphors was also discussed.

2. Experimental

$Sr_2(Ce_{1-x}Sn_x)O_4$ phosphors were prepared via a sol–gel route using citric acid and ethylene glycol as the chelating and polymerizing agents, respectively. Tin (IV) oxide was first dissolved in dilute hydrochloric acid. Stoichiometric amounts of analytical-grade strontium nitrate and cerium nitrate were then added into the above solution according to the composition of $Sr_2(Ce_{1-x}Sn_x)O_4$ ($0 \le x \le 0.07$). Citric acid was added into the above prepared solution and stirred for 1 h, followed by adding ethylene glycol. The molar ratio of citric acid to ethylene glycol was set at 1:1.5. The mixed solution was heated and stirred at 130 °C for 1.5 h to remove water. Further heating at 300 °C was performed to initiate the gelation reaction, in which citric acid chelated with the metal ions and reacted with ethylene glycol to form gels. The clear solution turned into a brownish gel as a result of gelation reaction. The gels were further heated at 500 °C in air for 3 h to remove organic residuals. The prepared precursors were then washed with deionized water, and the obtained powders were later heated at 1000 °C in air for 4 h.

The obtained powders were analyzed for phase purity using a diffractometer (Philips X'Pert) operated at 40 kV and 30 mA with Cu Kα radiation. Particle size analysis and morphological investigation of the prepared powders were performed using a field emission scanning electron microscope (FESEM) (Hitachi S-800) operated at 20 kV. Compositional analysis was carried out using an energy dispersive X-ray (EDX) spectroscope equipped on the FESEM (Hitachi S-800). Photoluminescence characteristics of the phosphors were determined by using a fluorescence spectrophotometer (Hitachi F-4500) using a 150 W Xe lamp as the excitation source at room temperature. The Commission International de l'Eclairage (CIE) analysis was performed by employing a fluorescence spectrophotometer (Hitachi F-4500) with an Ocean Optics CIE analyzer attachment. X-ray photoelectron spectroscopy (XPS)

* Corresponding author.
E-mail address: chlu@ntu.edu.tw (C.-H. Lu).

0925-8388/$ – see front matter © 2009 Elsevier B.V. All rights reserved.
doi:10.1016/j.jallcom.2009.06.154

was recorded using an X-ray photoelectron spectrometer (Thermo Scientific, Theta Probe) with a standard Al Kα (1486.68 eV) X-ray source.

3. Results and discussion

3.1. Characterization and microstructures of sol–gel derived $Sr_2(Ce_{1-x}Sn_x)O_4$ phosphors

$Sr_2(Ce_{1-x}Sn_x)O_4$ phosphors were prepared via the sol–gel process. With 1000 °C calcination for 4 h, well-crystallized powders were obtained. The X-ray diffraction patterns of $Sr_2(Ce_{1-x}Sn_x)O_4$ (x = 0, 0.01, 0.03, 0.05 and 0.07) are illustrated in Fig. 1. The patterns for all the samples were well consistent with the data in ICDD files (no. 89-5546) [14], and the structure of Sr_2CeO_4 was confirmed to be orthorhombic. When Sn^{4+} ions were doped to substitute cerium ions in the host lattice of $Sr_2(Ce_{1-x}Sn_x)O_4$ (x = 0.01, 0.03, 0.05 and 0.07), the crystallinity of the sample was found to slightly decrease as shown in Fig. 1(b)–(e). This may be due to the fact that the ionic radius of Ce^{4+} (0.087 nm for six-coordination) is larger than that of Sn^{4+} (0.069 nm for six-coordination) [15]. To measure the doping amount of Sn^{4+} in Sr_2CeO_4 host, EDX was performed in this study. The molar ratio of Sn^{4+}/Ce^{4+} in the prepared phosphors was found to monotonously increase with an increase in the doped Sn^{4+} concentration.

Fig. 2 shows the microstructures of the sol–gel derived $Sr_2(Ce_{1-x}Sn_x)O_4$ powders heated at 1000 °C for 4 h. In Fig. 2(a), the particle size of the sample (x = 0) was predominantly in the range of 0.3–0.8 μm. The morphology of the obtained powders with x = 0.03 and 0.07 was similar to that with x = 0, as evidenced in Fig. 2(b) and (c). However, the particles slightly enlarged with Sn^{4+} doping. In the sol–gel process, the metal ions are chelated with citric acid to form polymer networks due to polymerization reaction, which can help to reduce segregation of particular metal ions. Moreover, lower synthesis temperature and shorter heating time required in the sol–gel process, as compared with those of the solid-state reaction, both pose restrictive effects on the growth of $Sr_2(Ce_{1-x}Sn_x)O_4$ powders during calcination [16]. This probably explains why the sol–gel derived $Sr_2(Ce_{1-x}Sn_x)O_4$ powders were much smaller in particle size than the solid-state prepared powders (in the range of 7–27 μm) [17].

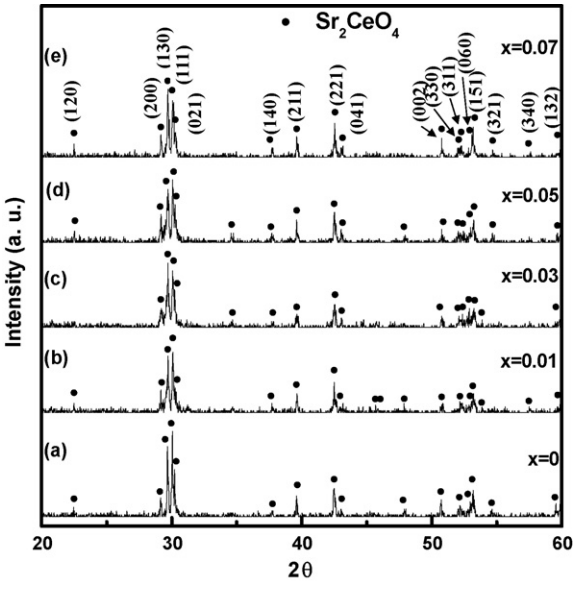

Fig. 1. X-ray diffraction patterns of $Sr_2(Ce_{1-x}Sn_x)O_4$ ($0 \le x \le 0.07$) phosphors calcined at 1000 °C for 4 h.

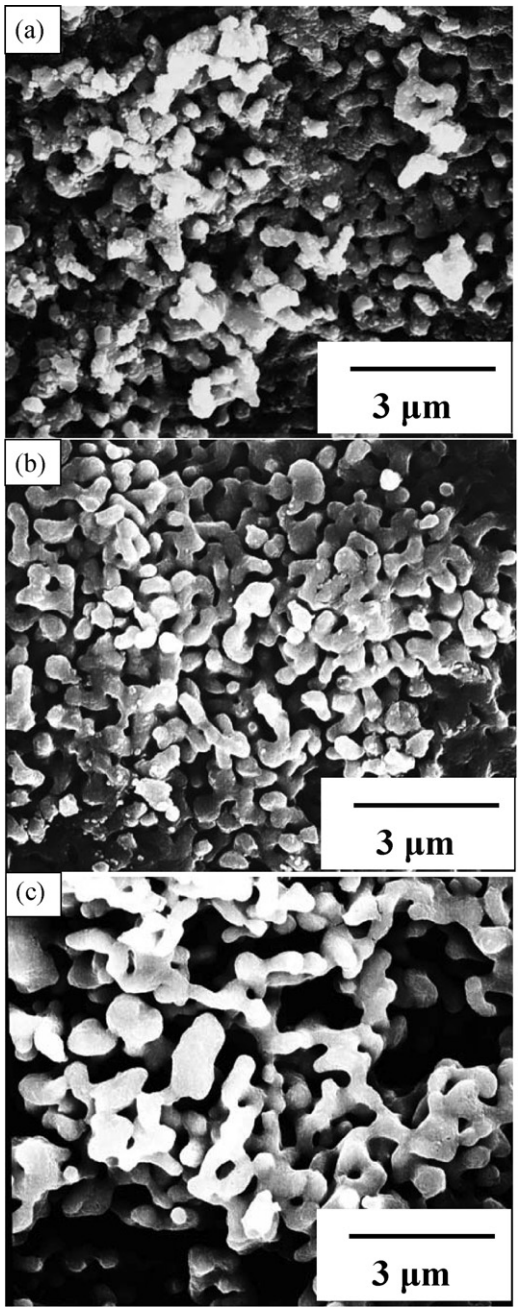

Fig. 2. Scanning electron microscopic images of $Sr_2(Ce_{1-x}Sn_x)O_4$ phosphors calcined at 1000 °C for 4 h: (a) x = 0, (b) x = 0.03, and (c) x = 0.07.

3.2. Luminescence properties of sol–gel derived $Sr_2(Ce_{1-x}Sn_x)O_4$ phosphors

The excitation spectra of the sol–gel derived $Sr_2(Ce_{1-x}Sn_x)O_4$ (x = 0, 0.01, 0.03, 0.05 and 0.07) phosphors are illustrated in Fig. 3. The excitation spectrum (λ_{em} = 483 nm) of Sr_2CeO_4 (x = 0) displays a broad absorption band in the UV region from 230 to 430 nm. It was noted that the excitation band was asymmetric and composed of two peaks at 294 and 344 nm, and this band could be assigned to the ligand-to-metal charge transfer from O^{2-} to Ce^{4+} [6]. An electron can transfer from an oxygen ligand to the empty 4f shell of Ce^{4+} ions under two conditions: in a low spin (LS) singlet excited state with no change in spin orientation (a spin-allowed transition, ΔS = 0), or in a high spin (HS) triplet excited state with change in spin orientation (a spin-forbidden transition, ΔS = 1). Based on Hund's rule, the

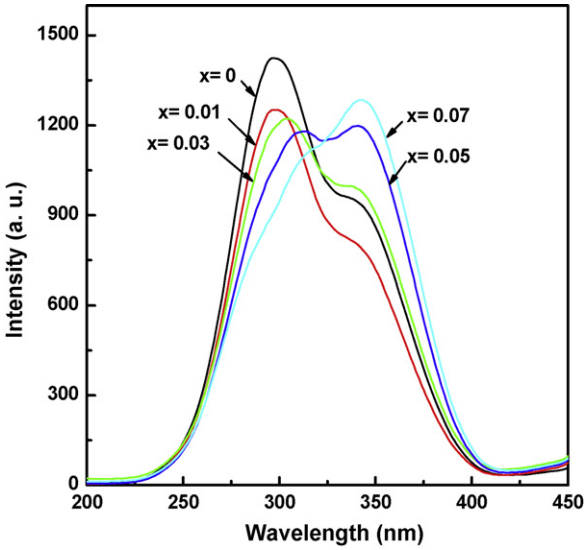

Fig. 3. Excitation spectra (λ_{em} = 483 nm) of $Sr_2(Ce_{1-x}Sn_x)O_4$ ($0 \le x \le 0.07$) phosphors calcined at 1000 °C for 4 h.

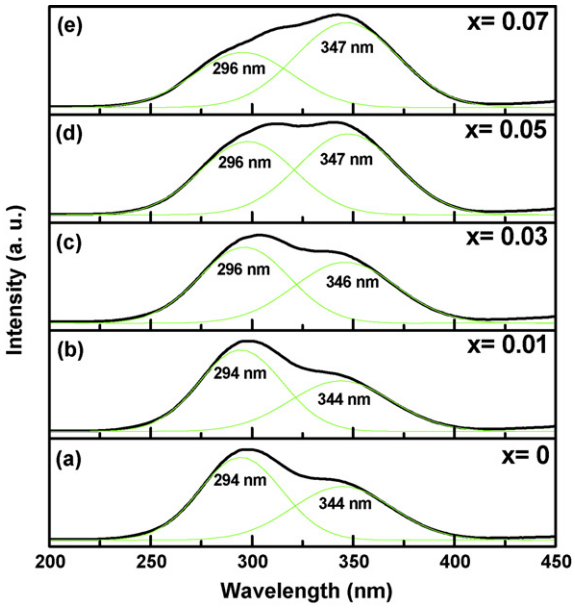

Fig. 4. De-convolution results of excitation spectra of $Sr_2(Ce_{1-x}Sn_x)O_4$ ($0 \le x \le 0.07$) phosphors calcined at 1000 °C for 4 h.

HS excited state is lower in energy than the LS excited state [9,18]. Accordingly, the high-energy (short wavelength) and low-energy (long wavelength) peaks could be assigned to the spin-allowed (LS) and spin-forbidden (HS) transitions, respectively.

When Sn^{4+} ions were doped into $Sr_2(Ce_{1-x}Sn_x)O_4$ phosphors, the excitation spectra changed significantly. As x was increased from 0.01 to 0.07, the intensity of the high-energy peak reversely decreased. It was also noted that the intensity of the low-energy peak increased with doping amount of Sn^{4+} ions. The enhanced excitation intensity of the low-energy peak is considered a result of weakened crystal field when increasing amount of Sn^{4+} ions were doped into the host. For an octahedron structure (such as CeO_6), the crystal field is markedly influenced by the ionic radii of the dopants and the nature of the metal ions [19]. Weak crystal field leads to more electrons transferring from the ground state to HS triplet excited state than to LS singlet excited state between Ce^{4+} 4f shell and oxygen ligands [20]. Thus, doping Sn^{4+} ions caused the enhancement in the excitation intensity of the low-energy peak. The highest excitation intensity of the low-energy peak was obtained as $x = 0.07$.

The asymmetric excitation spectra of $Sr_2(Ce_{1-x}Sn_x)O_4$ ($x = 0$, 0.01, 0.03, 0.05 and 0.07) phosphors were de-convoluted into two Gaussian peaks as shown in Fig. 4. In Fig. 4(a), the two peaks centering at 294 and 344 nm could be ascribed to the spin-allowed and spin-forbidden transitions, respectively. In $Sr_2(Ce_{1-x}Sn_x)O_4$ phosphors, the intensity of the high-energy peak (at around 294 nm) was higher than that of the low-energy peak (at around 344 nm) when the doping amount of Sn^{4+} ions was no more than $x = 0.03$ as shown in Fig. 4(a)–(c). The excitation bands of $Sr_2(Ce_{1-x}Sn_x)O_4$ ($x = 0.01$ and 0.03) and that of pure Sr_2CeO_4 phosphor showed similar patterns [8,21,22]. On the contrary, the intensity of the high-energy peak (at around 296 nm) was lower than that of the low-energy peak (at around 347 nm) when x was increased to 0.05 and 0.07. There are two probable explanations for the enhanced intensity of the low-energy peak: one is that more electrons transferred from the ground state to HS excited state than to LS excited state when the doping amount of Sn^{4+} ions was increased; the other is the existence of SnO_6 octahedron formed by replacing Ce^{4+} with Sn^{4+} in CeO_6 octahedron. A charge transfer in SnO_6 octahedron contributes to a broad excitation band at around 347 nm [23], which matches well with the position of the low-energy peak arisen from CeO_6 octahedron.

The high-energy and low-energy peaks were found to shift towards longer wavelength (from 294 to 296 nm and from 344 to 347 nm, respectively) when the doping amount of Sn^{4+} ions was increased from $x = 0$ to 0.07 as shown in Fig. 4. This observation could be ascribed to the lengthening of two types of Ce–O bonds in CeO_6 octahedron. As smaller Sn^{4+} ions were doped to substitute larger Ce^{4+} ions in the host, the formed Sn–O bonds were shorter in length than the original Ce–O bonds. This resulted in expansion of the neighboring CeO_6 octahedrons, leading to increased length of neighboring Ce–O bonds and thereby a red shift of the two excitation peaks.

Fig. 5 depicts the dependence of intensity ratio of the high-energy (high-E) excitation peak to the low-energy (low-E) one on the doping amount of Sn^{4+} ions. The ratio decreased with increasing amount of Sn^{4+} ions doped due to a change in the ligand

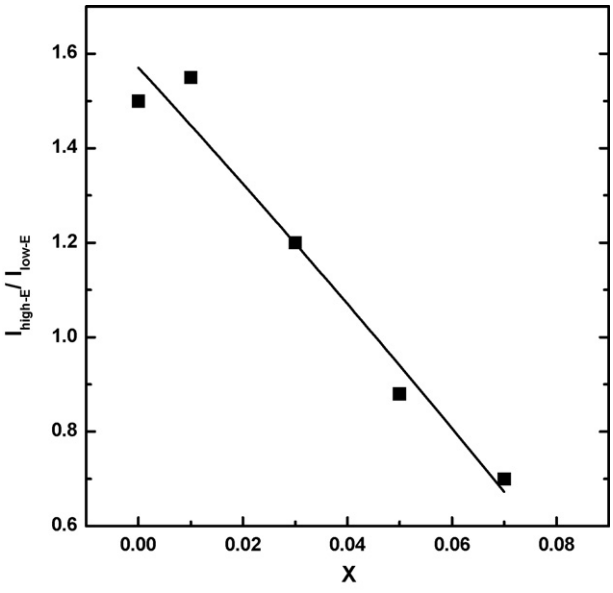

Fig. 5. Dependence of intensity ratio of the high-energy to low-energy excitation peaks on the doping amount of Sn^{4+} ions.

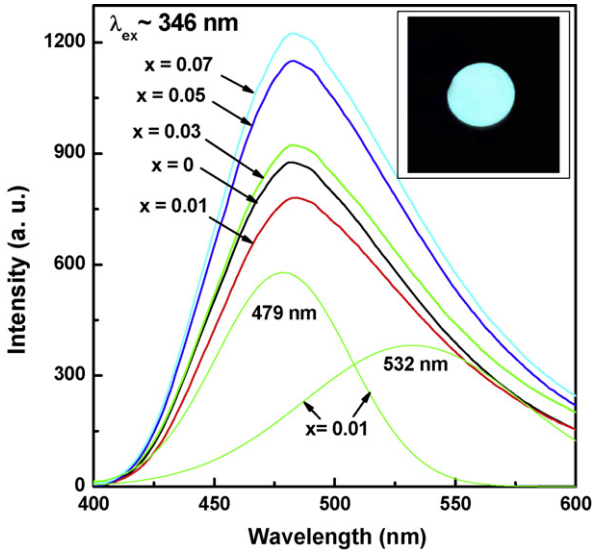

Fig. 6. Emission spectra ($\lambda_{ex} \sim 346$ nm) of $Sr_2(Ce_{1-x}Sn_x)O_4$ ($0 \le x \le 0.07$) phosphors calcined at 1000 °C for 4 h; the inset is the photograph of $Sr_2Ce_{0.93}Sn_{0.07}O_4$ phosphor upon UV excitation.

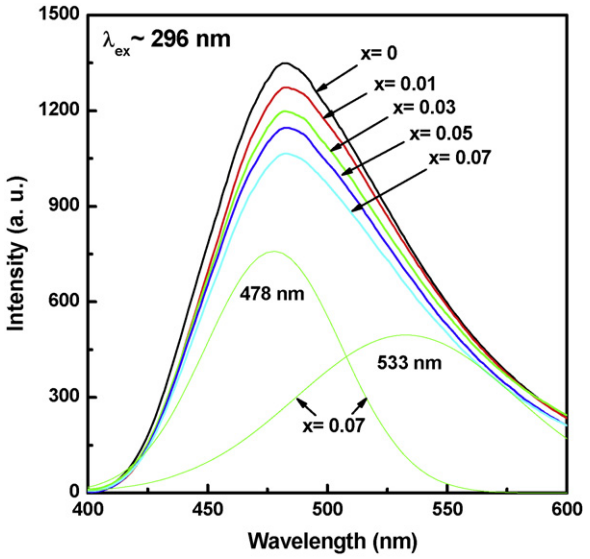

Fig. 7. Emission spectra ($\lambda_{ex} \sim 296$ nm) of $Sr_2(Ce_{1-x}Sn_x)O_4$ ($0 \le x \le 0.07$) phosphors calcined at 1000 °C for 4 h.

environment, indicating the feasibility of fine tuning the excitation spectra of $Sr_2(Ce_{1-x}Sn_x)O_4$ phosphors by adjusting the doping amount of Sn^{4+} ions.

The emission spectra (monitored at the wavelength of low-energy excitation peak) of the sol–gel derived $Sr_2(Ce_{1-x}Sn_x)O_4$ ($x = 0$–0.07) phosphors doped with various amounts of Sn^{4+} ions are shown in Fig. 6. When $x = 0$, a broad emission band peaking at 483 nm was observed. As the doping amount of Sn^{4+} ions was increased to 0.01, the emission intensity adversely decreased due to a decrease in the crystallinity of the sample. When the doping amount of Sn^{4+} ions was further increased to 0.07, the emission intensity of the sample greatly increased by 139% as compared to that of undoped Sr_2CeO_4 phosphor upon excitation at 346 nm. The observed emission band for every sample was assigned to the metal-to-ligand charge transfer (MLCT) transition [24]. The emission band was asymmetric and composed of two Gaussian peaks centering at 479 and 532 nm, and these two peaks were resulted from two charge transfer transitions with different energy levels because of two different lengths of Ce–O bonds in CeO_6 octahedron [24]. The structure of Sr_2CeO_4 consists of linear chains of edge-sharing CeO_6 octahedron, and the notable feature of the chains is the presence of two trans terminal Ce–O groups perpendicular to the plane defined by four equatorial μ^2–O atoms. The terminal Ce–O bonds are about 0.1 Å shorter than the equatorial bonds [6], thereby leading to charge transfer transition with different energy levels because of the two types of Ce–O bonds. The energies of terminal and equatorial metal-to-ligand excited states lie at 2.59 eV ($\lambda_{em} = 479$ nm) and 2.33 eV ($\lambda_{em} = 532$ nm) above the ground state, respectively. The Commission International de l'Eclairage (CIE) chromaticity coordinates for Sn^{4+}-doped Sr_2CeO_4 phosphors were recorded. Since the emission spectra of the prepared samples showed no shift with various amounts of doped Sn^{4+}, the chromaticity coordinates for all the prepared samples were the same. The measured coordinate was at (0.18, 0.26). The photograph of $Sr_2Ce_{0.93}Sn_{0.07}O_4$ phosphor excited by an UV light source is shown in the inset of Fig. 6 and its corresponding emission intensity was the highest among all the samples.

The emission spectra (monitored at 296 nm) of the sol–gel derived $Sr_2(Ce_{1-x}Sn_x)O_4$ phosphors are shown in Fig. 7. When $x = 0$, a broad emission band peaking at 483 nm was observed. As x was increased from 0.01 to 0.07, the emission intensity gradually decreased due to the decrease in the excitation intensity at 296 nm. This reduction in emission intensity was mainly ascribed to more electrons transferring from the ground state to HS excited state than to LS excited state when Sn^{4+} ions were doped into Sr_2CeO_4 matrix.

The excitation and emission bands for $Sr_2(Ce_{1-x}Sn_x)O_4$ phosphors were ascribed to the charge transfer between O^{2-} and Ce^{4+}. However, Ce^{3+} ion is a well-known activator, which was used in various phosphor systems for producing blue emission under suitable excitation energy [25]. Therefore it is necessary to make sure if there is Ce^{3+} on the surface of the phosphors. Fig. 8 depicts the XPS spectra of $Sr_2(Ce_{1-x}Sn_x)O_4$ ($x = 0$–0.07) phosphors for Ce (3d). For all the samples, the peaks at 881.8, 888.4, 898.1, 900.5, 906.8 and 916.4 were all assigned to Ce^{4+} ion without the detection of Ce^{3+} ions [9,26], indicating that the excitation and emission bands for $Sr_2(Ce_{1-x}Sn_x)O_4$ phosphors were completely ascribed to the ligand-to-metal and metal-to-ligand charge transfers, respectively.

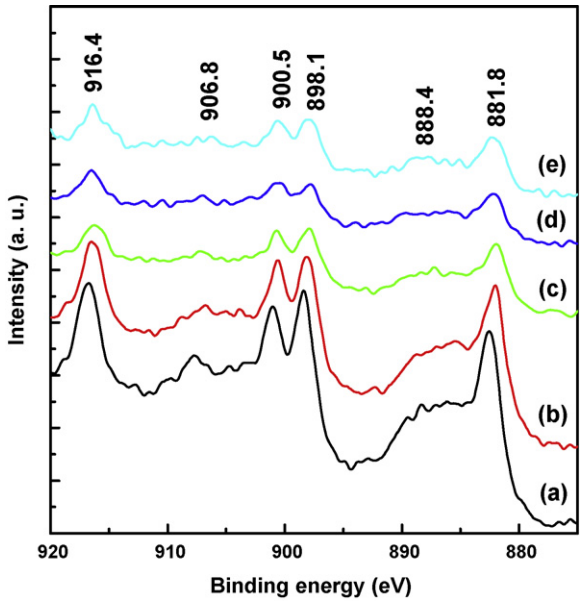

Fig. 8. X-ray photoelectron spectroscopy of $Sr_2(Ce_{1-x}Sn_x)O_4$ phosphors ((a) $x = 0$; (b) $x = 0.1$; (c) $x = 0.3$; (d) $x = 0.5$; (e) $x = 0.7$) for Ce (3d).

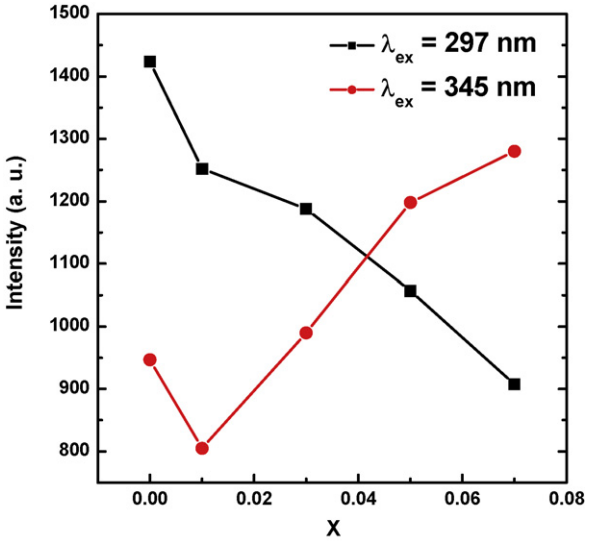

Fig. 9. Dependence of emission intensity of $Sr_2(Ce_{1-x}Sn_x)O_4$ ($x = 0.07$) phosphors excited at 297 and 345 nm on the doping amount of Sn^{4+} ions.

Fig. 9 demonstrates the dependence of emission intensity of $Sr_2(Ce_{1-x}Sn_x)O_4$ ($x = 0$–0.07) phosphors excited at 297 nm (high-energy peak of excitation spectra) and 345 nm (low-energy peak of excitation spectra) on the amount of Sn^{4+} ions doped. As discussed above in Fig. 6, the emission intensity of the sample excited at 346 nm reduced owing to a decrease in crystallinity when the doping amount of Sn^{4+} ions was increased to 0.01, and the emission intensity further raised by 139% as compared to that of undoped Sr_2CeO_4 phosphor when the doping amount of Sn^{4+} was increased to 0.07. On the other hand, when the samples were excited at the wavelength of high-energy peak (297 nm), the emission intensity decreased with increasing doping amount of Sn^{4+} since doping Sn^{4+} into the host led to weakened crystal field. Moreover, most electrons were expected to transfer from ground state to the low-energy excited state (HS triplet excited state) instead of transferring to the high-energy one (LS singlet excited state). Conclusively, blue emission of the phosphors upon excitation at 346 nm can be enhanced by doping Sn^{4+} ions into Sr_2CeO_4 host.

3.3. Band structure of sol–gel derived $Sr_2(Ce_{1-x}Sn_x)O_4$ phosphors

Based on the recorded excitation and emission spectra, the band structure of $Sr_2(Ce_{1-x}Sn_x)O_4$ ($x = 0.07$) phosphor and the energy level distribution within the band gap were illustrated in Fig. 10. Once the phosphors are irradiated, the electrons jump from valence band (VB) to excited states with and without a change in spin orientation (HS and LS charge transfer state (CTS), respectively). The excitation spectrum of $Sr_2(Ce_{0.03}Sn_{0.07})O_4$ phosphor consisted of two peaks at 296 and 347 nm, which are assigned to the transition from ground state to LS and HS CTS, respectively. Therefore, the LS CTS is supposed to locate at 4.19 eV above the VB. The HS CTS is located at 3.57 eV, which is lower in energy than that of LS CTS since the transition between HS CTS and VB is parity forbidden [23]. After the excitation, the excited electrons release from LS and HS CTS to two MLCT states via a non-radiative process. The $(MLCT)_{terminal}$ state is higher in energy than that of $(MLCT)_{equatorial}$ due to the difference in length between terminal and equatorial Ce–O bonds in CeO_6 octahedron. The emission bands at 479 and 532 nm were ascribed to the transition from MLCT states ($(MLCT)_{terminal}$ lies at 2.59 eV and $(MLCT)_{equatorial}$ at 2.33 eV as shown in Fig. 8) to VB. In comparison, the energy levels of LS and HS states of this sample were both lower than those of Sr_2CeO_4 phosphor without Sn^{4+} doping. This observation can be ascribed to the red shift of the excitation peaks because of lengthened Ce–O bonds as Sn^{4+} ions were doped.

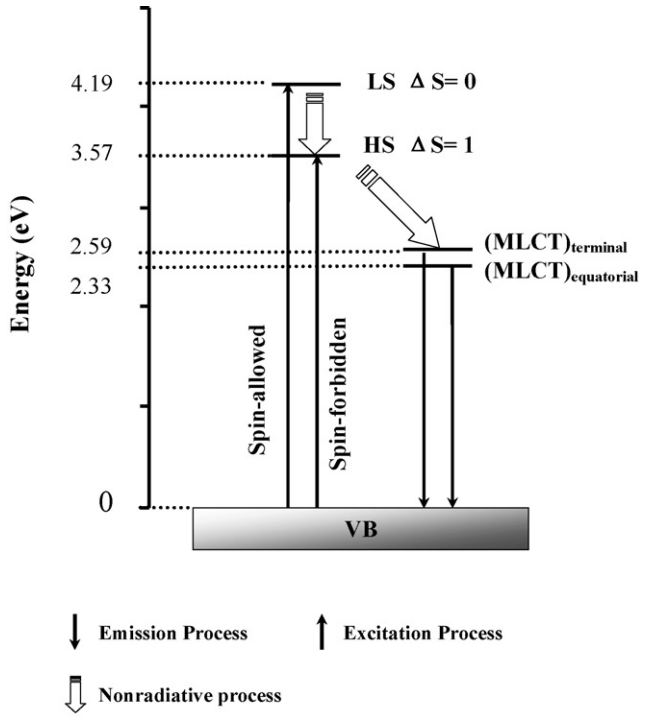

Fig. 10. Schematic diagram of the energy levels in $Sr_2(Ce_{1-x}Sn_x)O_4$ ($x = 0.07$) phosphors.

4. Conclusions

$Sr_2(Ce_{1-x}Sn_x)O_4$ phosphors were successfully synthesized via the sol–gel route. The prepared phosphors displayed asymmetric excitation spectra which composed of two broad bands at around 296 and 346 nm. As Sn^{4+} ions were doped, the excitation intensity at 346 nm was enhanced, and the ratio of the intensity at 346 nm to that at 296 nm was also increased. The variation in the intensity ratio was attributed to a reduction in the crystal field in $Sr_2(Ce_{1-x}Sn_x)O_4$ host. Additionally, a red shift in the excitation spectra of $Sr_2(Ce_{1-x}Sn_x)O_4$ phosphors occurred because of the lengthening of Ce–O bonds. $Sr_2(Ce_{1-x}Sn_x)O_4$ phosphors produced blue emission at 483 nm upon excitation at 296 and 346 nm. The doping of Sn^{4+} ions was found to remarkably enhance the emission intensity of the phosphors excited at 346 nm.

References

[1] L. Muresan, E.-J. Popovici, R. Grecu, L.B. Tudoran, J. Alloys Compd. 471 (2009) 421.
[2] R. Ghildiyal, P. Page, K.V.R. Murthy, J. Lumin. 124 (2007) 217.
[3] C.H. Lu, R. Jagannathan, Appl. Phys. Lett. 80 (2002) 3608.
[4] S.S. Yi, K.S. Shim, H.K. Yang, B.K. Moon, B.C. Choi, J.H. Jeong, J.H. Kim, J.S. Bae, Appl. Phys. A 87 (2007) 667.
[5] L. Zhou, J. Wei, J. Wu, F. Gong, L. Yi, J. Huang, J. Alloys Compd. 476 (2009) 390.
[6] E. Danielson, M. Devenney, D.M. Giaquinta, J.H. Golden, R.C. Haushalter, E.W. McFarland, D.M. Poojary, C.M. Reaves, W.H. Weinberg, X.D. Wu, Science 279 (1998) 837.
[7] E. Danielson, M. Devenney, D.M. Giaquinta, J.H. Golden, R.C. Haushalter, E.W. McFarland, D.M. Poojary, C.M. Reaves, W.H. Weinberg, X.D. Wu, J. Mol. Struct. 470 (1998) 229.
[8] X.M. Liu, Y. Luo, J. Lin, J. Crystal Growth 290 (2006) 266.
[9] T. Masui, T. Chiga, N. Imanaka, G. Adachi, Mater. Res. Bull. 38 (2003) 17.
[10] D.S. Xing, M.L. Gong, X.Q. Qiu, D.J. Yang, K.W. Cheah, J. Rare Earth 24 (2006) 289.
[11] X. Li, Z. Yang, L. Guan, Q. Guo, C. Liu, P. Li, J. Alloys Compd. 464 (2008) 565.
[12] K.Y. Jung, J.H. Seo, Electrochem. Solid State Lett. 11 (2008) J64.
[13] T. Nishida, T. Ban, N. Kobayashi, Appl. Phys. Lett. 82 (2003) 3817.
[14] ICDD Powder Diffraction File, card no. 89-5546.

[15] Y.M. Chiang, Physical Ceramics: Principles for Ceramics Science and Engineering, Wiley, USA, 1997, p. 15.
[16] M. Kakihana, M. Yoshimura, Bull. Chem. Soc. Jpn. 72 (1999) 1427.
[17] R. Sankar, G.V. Subba Rao, J. Electrochem. Soc. 147 (2000) 2773.
[18] L. van Pieterson, S. Soverna, A. Meijerink, J. Electrochem. Soc. 147 (2000) 4688.
[19] S. Shionoya, W.M. Yen, Phosphor Handbook, CRC Press, New York, 1998.
[20] G.L. Miessler, D.A. Tarr, Inorganic Chemistry, 3rd edition, Pearson Prentice Hall, 2004.
[21] J. Gomes, A.M. Pires, O.A. Serra, Quim. Nova 27 (2004) 706.
[22] C.H. Lu, C.T. Chen, J. Sol–Gel Sci. Technol. 43 (2007) 179.
[23] Y.C. Chung, Y.H. Chang, B.S. Tsai, J. Alloys Compd. 398 (2005) 256.
[24] A. Nag, T.R.N. Kutty, J. Mater. Chem. 13 (2003) 370.
[25] L.Y. Cai, X.D. Wei, H. Li, Q.L. Liu, J. Lumin. 129 (2009) 165.
[26] S.J. Chen, X.T. Chen, Z. Yu, J.M. Hong, Z. Xue, X.Z. You, Solid State Commun. 130 (2004) 281.